chemistry

MDPI

Article

Effect of Hydrazine Pretreatment on the Activity, Stability and Active Sites of Cobalt Species for Preferential Oxidation (PROX) of CO in H_2-Rich Stream

Reineck Mhlaba [1], Thuto Mosuang [2] and Takalani Magadzu [1,*]

[1] Faculty of Science and Agriculture, School of Physical and Mineral Science, Department of Chemistry, University of Limpopo, Private Bag x1106, Sovenga 0727, South Africa; reineck.mhlaba@ul.ac.za

[2] Faculty of Science and Agriculture, School of Physical and Mineral Science, Department of Physics, University of Limpopo, Private Bag x1106, Sovenga 0727, South Africa; thuto.mosuang@ul.ac.za

* Correspondence: Takalani.magadzu@ul.ac.za

Received: 8 August 2019; Accepted: 15 October 2019; Published: 22 October 2019

Abstract: The as-prepared (Co_3O_4) and hydrazine-treated (Co_3O_4(H)) cobalt catalysts were prepared using the precipitation method and evaluated at a temperature range of 40–220 °C for preferential oxidation (PROX) of CO in excess hydrogen. An improved surface reducibility with smaller crystallite size was noted on hydrazine-treated cobalt species (i.e., Co_3O_4(H) catalyst), which indicates some surface transformation. This finding correlates with the surface roughness formation (as depicted by scanning electron microscope (SEM) and transmission electron microscope (TEM) data), which was further confirmed by an increase in the Brunauer–Emmett–Teller (BET) surface area. The mesoporous structure of the Co_3O_4(H) catalyst remained intact, as compared to that of the Co_3O_4 catalyst. Interestingly, the in situ treatment of the standalone Co_3O_4(H) catalyst decreased the maximum CO conversion temperature ($T_{100\%}$) from 160 °C (over Co_3O_4) to 100 °C, with good selectivity. The Co_3O_4(H) catalyst showed good stability, with approximately 85% CO conversion at 100 °C for 21 h, as compared to a faster deactivation of the Co_3O_4 catalyst. However, the Co_3O_4(H) catalyst was unstable in both CO_2 and the moisture environment. Based on the evaluation of spent hydrazine-treated (CoO(H)) cobalt catalyst, the high PROX activity is associated with the formation of Co^{3+} species as confirmed by X-ray diffraction (XRD), X-ray photoelectron spectra (XPS), and temperature-programmed reduction (TPR) data.

Keywords: PROX; Co_3O_4; CoO(H); Co_3O_4(H); catalyst; CO conversion and selectivity

1. Introduction

The adoption of hydrogen (H_2) proton exchange membrane (PEM) fuel cells as source of energy of the future can mitigate the impact of carbon emission to the environment [1]. PEM fuel cells are fueled with H_2 that is generally produced by steam reformation of methanol, and the produced gas generally contains about 1% CO, which can poison the anode terminal [2,3]. The preferential oxidation (PROX) reaction has attracted much attention because of its potential applications in selectively oxidizing CO, reducing its concentration to less than 10 ppm without oxidation of excess hydrogen present [2–4].

A variety of noble metal-supported catalysts such as Pd, Pt [5–7], and nano Au [8,9] are promising for CO PROX reaction. However, some of these catalysts are mainly active at a higher temperature range (150–300 °C) with a lower selectivity to CO_2 and are not cost-effective as compared to a variety of metal oxides. Furthermore, previous studies have shown that platinum group metals (PGMs) decrease the activity of the metal oxide catalysts on CO PROX [5,10–12]. For example, Nguyen et al. [10] reported higher selectivity of H_2 oxidation at a low temperature on a Pt surface than on Co_3O_4, due to

a lower dissociation barrier of H_2 on the Pt surface. Other researchers have shown that supported Pd species suppress CO PROX activity due to the formation of β-hydrides (which promotes moisture formation and lower CO conversion) [11,13]. Supported metal oxide catalysts such as CuO/CeO_2 have shown good PROX activity (approximately 100% CO conversion) at temperatures ranging from 110 to 160 °C [14–17].

However, cobalt-based catalysts such as CoO and Co_3O_4 (as standalone catalysts) have recently attracted a significant amount of interest from the scientific community, due to their promising activities in the absence [18] and presence of hydrogen [19,20]. The former (CoO) has exhibited good catalytic activities in PROX reaction (in excess H_2) over a wide temperature range, as compared to other transition metal oxides [19]. Such PROX activity was reported to be influenced by the tetrahedrally coordinated Co^{2+} species [19], although no supporting evidence was provided. In the absence of hydrogen, the high CO oxidation activity is attributed to the surface oxidation of octahedrally coordinated Co^{2+} species within the CoO structure [18]. Although the view of Co^{3+} as an active site for CO oxidation over Co_3O_4 has long been reported through density function theory (DFT) studies [21] and recently confirmed by X-ray absorption spectroscopy (XAS), near-ambient pressure X-ray photoelectron spectra (NAP-XPS), SEM, TEM, and FTIR methods [20,22], this metal oxide was able to achieve 50% conversion, with relatively low selectivity under PROX reaction at approximately 100 °C [18,19]. Furthermore, the catalyst deactivates due to surface reconstruction, which hinders the redox cycle [23]. For the PROX catalysts to operate effectively, the catalyst has to start working at room temperature and achieve higher activity and selectivity at approximately 80–100 °C [24].

A variety of prepared metal oxide-supported catalysts have shown that pretreatment conditions play a crucial role towards the formation of desired species and improved activities. For example, previous [25] and recent reports [26,27] have indicated an improved CO oxidation activity of a catalyst upon pretreatment with a reducing agent. In addition, a recent report indicated that the purity of the prepared Co_3O_4 phase plays a crucial role toward high CO oxidation [22]. Such a variety of factors have never been considered on metal oxide catalysts such as Co_3O_4 alone, towards PROX reaction. Hence, the study was aimed at investigating the effects of pretreatment of $Co(OH)_2$ species using hydrazine (N_2H_4) prior to formation of Co_3O_4 by calcination; and comparing with existing methods of just calcining the $Co(OH)_2$ at a specific temperature. The role of cobalt oxidation states and structure of as-prepared and spent catalysts was investigated to elucidate the correlation with the observed catalytic activities. Furthermore, the catalytic stability of the catalysts on PROX of CO in a dry, moisture, and CO_2 atmosphere was evaluated for 21 h on stream at 100 °C.

2. Experimental Section

2.1. Preparation of Catalysts

A variety of Co_3O_4 catalysts were prepared using the precipitation method following the procedure reported by Chen et al. [28], with modification. Briefly, the required amount of cobalt nitrate hexahydrate ($Co(NO_3)_2$. $6H_2O$, Sigma Aldrich) was added to 100 mL distilled water and stirred for 30 min at room temperature. Thereafter, 62 mL of 2 M sodium hydroxide (NaOH) solution was added dropwise with vigorous stirring until pH 12 was reached. The mixture was stirred for 3 h at 70 °C and allowed to digest for 1 h at room temperature. The resulting precipitates were filtered through suction filtration and thoroughly washed with warm distilled water. The as-prepared $Co(OH)_2$ precipitates were dried at 80 °C for 24 h.

A portion of the precipitates were calcined in air at 300 °C for 4 h to form the Co_3O_4. The remaining precipitates of $Co(OH)_2$ were re-dispersed in 20 mL distilled water. Then, 100 mL of 0.1 M hydrazine hydrate ($N_2H_4{\cdot}H_2O$) solution was added dropwise and stirred for 15 h at room temperature [27]. The resulting solid was collected through centrifugation, washed with distilled water, and dried at 80 °C for 24 h. A portion of the solid formed which consists of a mixture of $Co(OH)_2$ and CoO(OH) (denoted as CoO_xH_y(H)) [29] was calcined at 300 °C in air for 4 h to form a Co_3O_4(H) catalyst.

For comparison, a mesoporous hydrazine-treated CoO was prepared by reducing the Co_3O_4(H) in a mixture of 5% H_2 balanced helium at 250 °C for 1.5 h (600 mg Co_3O_4, 30 mL·min^{-1}) [18]. A simplified representation of the synthetic process of all catalysts is illustrated in Scheme 1 below.

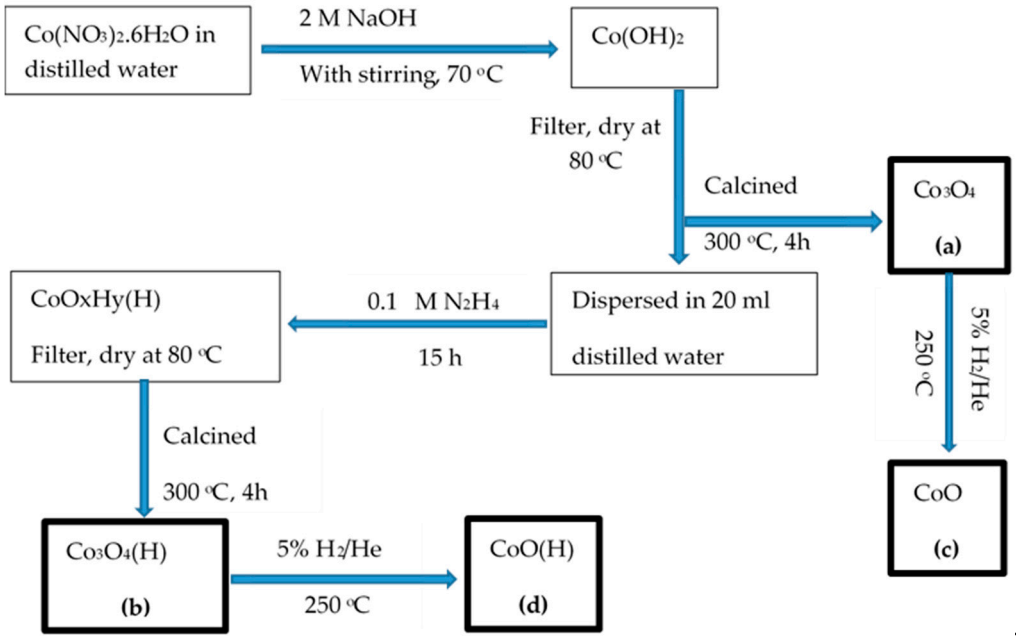

Scheme 1. Schematic representation of the synthetic strategy of (a) Co_3O_4, (b) Co_3O_4(H), (c) CoO, and (d) CoO(H) catalysts.

2.2. Characterisation of Catalysts

The morphologies of the samples were observed using a JEOL JSM-5410V scanning electron microscope (SEM) operating at an accelerated voltage of 15 kV. Transmission electron microscope (TEM) images were obtained using the TECNAI 20 TWIN electron microscope operated at 120 kV. Powder X-ray diffraction (XRD) patterns were recorded on a Philips Analytical Powder X-ray B.V. (Philips, Holland), PW3710 based diffractometer, with graphite monochromatized Cu–Kα radiation (40 KV, 40 mA). The crystal diameter of cobalt species was estimated from the Scherrer equation using the (311) plane diffraction peak. The Brunauer–Emmett–Teller (BET) specific surface areas of the samples were measured via N_2 adsorption at −196 °C on a Micromeritics tristar II 3020 system. Before the measurements, samples were degassed under air at 200 °C for 2 h. Thermogravimetric analysis (TGA) was carried out at a heating rate of 10 °C/min from ambient temperature to 600 °C under N_2 with a flow rate of 40 mL/min using an STA Perkin-Elmer 4000 (PerkinElmer, Waltham, MA, USA). The Fourier transform infrared spectroscopy (FTIR) spectra of the samples were recorded using a Spectrum II spectrophotometer (PerkinElmer, Waltham, MA, USA).

The X-ray photoelectron spectra (XPS) were acquired with an ESCA-3400 spectrometer (Shimadzu Co. Ltd) equipped with a Mg K X-ray exciting source (1253.6 eV) operating at 10 kV and 10 mA. All the elemental binding energies were referenced to the C (1s) line situated at 285.0 eV. Hydrogen temperature-programmed reduction (H_2-TPR) of the samples were carried out on a Micromeritiscs Autochem II 2920 equipped with a thermal conductivity detector (TCD). The TPR analysis was started by conditioning approximately 0.035 g of a sample under a flow of 10% O_2/Helium gas for 1 h. The TPR analysis was carried by flowing a 10% H_2/Argon gas through the samples, while the temperature was raised linearly from room temperature to 900 °C at a heating rate of 10 °C/min.

2.3. Catalytic Activity Tests

The catalysts were tested at atmospheric pressure for PROX of CO using a U-shape fixed bed reactor (inner diameter of ~0.5 cm). Samples of catalysts (~200 mg) were placed in a quartz reactor and heated at 40 °C under helium for 30 min at a flow rate of 20 mL·min^{-1}. Afterward, the catalysts were brought into contact with the feed composed of 1% CO, 1% O_2, and 50% H_2, balanced with He, at a total flow rate of 100 mL·min^{-1} (equivalent to weight hourly space velocity of 30,000 mL·h^{-1}.g^{-1}). The reactor temperature was monitored using a K-type thermocouple fitted close to the catalyst bed. A moisture trap consisting of dehydrated copper sulphate was installed before gas chromatography (GC) to remove moisture formed during the reaction. The reactants and reaction products were separated by a Porapack-Q (50/20 mesh, 1/8 × 1.5 m) and the molecular sieve 5A (1.5 m) columns and analyzed through online gas chromatography (DANI-GC) equipped with a thermal conductive detector (TCD).

The CO conversion (Equation (1)) as well as the selectivity (Equation (2)) towards CO_2 and (Equation (3)) H_2O were calculated using the following equations:

$$x_{CO} = \frac{[CO]_{in} - [CO]_{out}}{[CO]_{in}} \times 100\% \quad (1)$$

$$s_{CO_2} = 0.5 \times \left(\frac{[CO]_{in} - [CO]_{out}}{[O_2]_{in} - [O_2]_{out}} \right) \times 100\% \quad (2)$$

$$s_{H_2O} = 0.5 \times \left(\frac{[H_2]_{in} - [H_2]_{out}}{[O_2]_{in} - [O_2]_{out}} \right) \times 100\% \quad (3)$$

where $[CO]_{in}$, $[H_2]_{in}$, and $[O_2]_{in}$ are the inlet concentrations of CO, H_2, and O_2, respectively; and $[CO]_{out}$, $[H_2]_{out}$, and $[O_2]_{out}$ are the outlet concentrations of CO, H_2, and O_2, respectively.

3. Results and Discussion

3.1. Thermal and Structural Properties of Catalysts

Figure 1 shows the XRD patterns of $Co(OH)_2$, CoO_xH_y(H), Co_3O_4, Co_3O_4(H), CoO(H), and spent CoO(H) catalysts. The XRD profile of CoO_xH_y(H) shows overlapping peaks at 2θ values of 20 and 39° (Figure 1b). This confirms that a transformation process from $Co(OH)_2$ to CoO(OH) phases has occurred [29] due to the oxidation of $Co(OH)_2$ (Figure 1a). The XRD profile of Co_3O_4 (Figure 1c) reveals the diffraction peaks at 2θ values of 19.2, 31.2, 36.6, 38.9, 45.1, 55.7, and 59.5° that are assigned to (111), (220), (311), (222), (400), (422), and (511) crystal planes, respectively [30–33]. The crystal planes are in good agreement with the cubic spinel type Co_3O_4 phase (JCPDS Card No. 76-1802) [34–36].

Interestingly, the peak intensity at 36.6° 2θ of Co_3O_4(H) (Figure 1d) has decreased substantially as compared to the Co_3O_4 sample (Figure 1c). This peak decrease indicates the formation of smaller crystallite sizes of the Co_3O_4 phase, as estimated using Scherrer's equation. This clearly suggests that some surface rearrangements have occurred, as evidenced by an increase in its surface area (62.2 m^2/g) (Table 1). This finding correlates with the surface roughness formation as depicted by SEM and TEM data. The data correlate with the reported improved surface area of Co_3O_4, upon calcination of CoO(OH) [29]. The nitrogen adsorption–desorption isotherm data further indicate an increase in the porosity and pore volume of Co_3O_4(H) (Table 1) following in situ reduction. The mesoporous nature of Co_3O_4(H) phase remained intact, which is in agreement with the results reported by Li et al. [27] on mesoporous CeO_2 support.

In order to evaluate the role of Co^{3+} species on PROX reaction, a CoO(H) was prepared by pretreating the Co_3O_4(H) by 5% H_2 at 250 °C [18]. The prepared CoO(H) (Figure 1e) was indeed confirmed by the presence of two prominent XRD peaks at 2θ values of 36.6 and 42.7° [18]. The XRD data of spent CoO(H) (Figure 1f) show the re-emergence of a (200) plane (which is the characteristic

profile of Co_3O_4) upon using the catalyst in PROX of CO. This clearly supports the notion that Co^{2+} species is transformed into Co^{3+} species during PROX reaction as noted elsewhere [18].

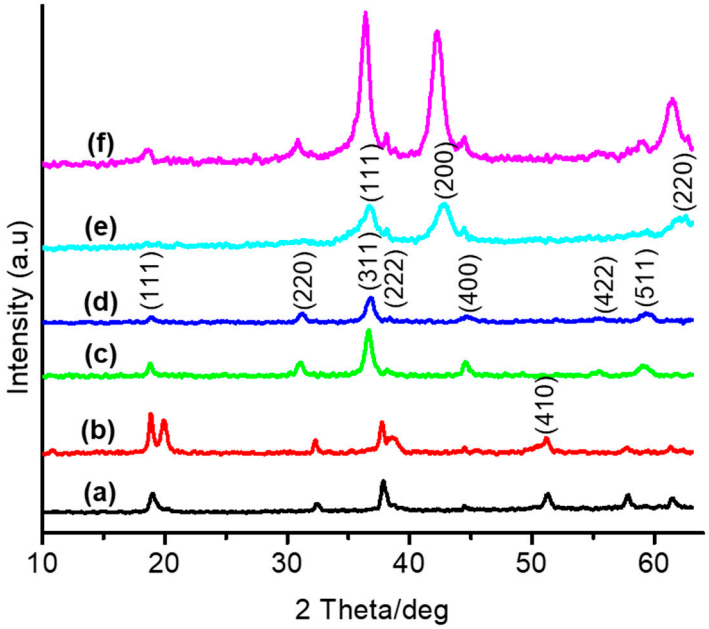

Figure 1. The XRD patterns of (a) $Co(OH)_2$, (b) CoO_xH_y(H), (c) Co_3O_4, (d) Co_3O_4(H), (e) CoO(H), and (f) spent CoO(H) catalyst.

Table 1. The effect of pretreatment on the crystallite size and surface area of the as-prepared samples.

Catalyst	S_{BET} (m^2/g)	Pore Volume ($cm^3 \cdot g^{-1}$)	Pore Size (nm)	Average Crystallite Size (nm) [a]	T_{max} (°C) [b]	Maximum CO Conversion (%) [b]
Co_3O_4(H)	62.2	0.158	9.95	20.0	120	98.1
CoO(H)	56.6	0.184	13.0	11.4	140	98.5
Co_3O_4	49.7	0.137	11.3	23.2	160	96.7

[a] Average crystallite sizes were estimated from the (311) plane of XRD patterns. [b] T_{max} is the temperature achieving the maximum CO conversion. Reaction conditions: 1% CO, 1% O_2, and 50% H_2, balanced with He, at a total flow rate of 100 $mL \cdot min^{-1}$ (equivalent to weight hourly space velocity of 30,000 $mL \cdot h^{-1} \cdot g^{-1}$).

The stability of formed CoO_xH_y(H), Co_3O_4, Co_3O_4(H), and CoO(H) catalysts were investigated by means of TGA under a nitrogen gas atmosphere at a heating rate of 10 °C/min, as shown in Figure 2. The TGA profile of CoO_xH_y(H) (Figure 2a) show loss of water and oxygen molecules (~12.3%) starting from 240 °C, which indicates transformation to Co_3O_4. Similar behaviors were reported elsewhere [37,38], during the transformation of CoO(OH)/$Co(OH)_2$ to Co_3O_4 in the presence of ambient air/helium. However, the Co_3O_4 (Figure 2b) and Co_3O_4(H) (Figure 2c) samples remained relatively stable up to 600 °C. This clearly indicates that the calcination process undertaken after in situ reduction completely transformed all cobalt species to a spinel Co_3O_4 phase. The TGA profile of CoO(H) initially showed a weight loss of 3.6% at 100 °C (the catalyst was not pretreated prior to analysis, and hence, the weight loss is due to the presence of moisture) (Figure 2d) which remained relatively stable up to 600 °C.

The XPS data in Figure 3 show the Co 2p spectra of Co_3O_4, Co_3O_4(H), and CoO(H) catalysts. Two prominent peaks (at approximately 780.8 and 796.2 eV) with the absence of satellite peak at 786 eV are due to the presence of Co^{3+} and Co^{2+} species within the Co_3O_4 spinel (Figure 3Ba,b) [39,40]. The XPS data of CoO(H) was confirmed by the presence of a small satellite peak at 786 eV (Figure 3Bc). However, the XPS data of Co_3O_4(H) (Figure 3Bb) catalysts show similar features as those of Co_3O_4 (Figure 3Ba), which indicates that treatment with hydrazine did not alter/lower the oxidation state.

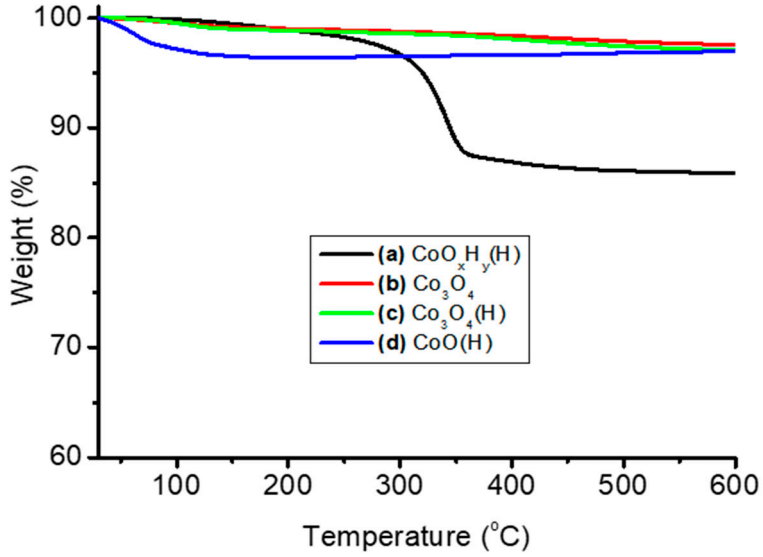

Figure 2. Thermogravimetric analysis of (a) $CoO_xH_y(H)$, (b) Co_3O_4, (c) $Co_3O_4(H)$, and (d) CoO(H) catalysts.

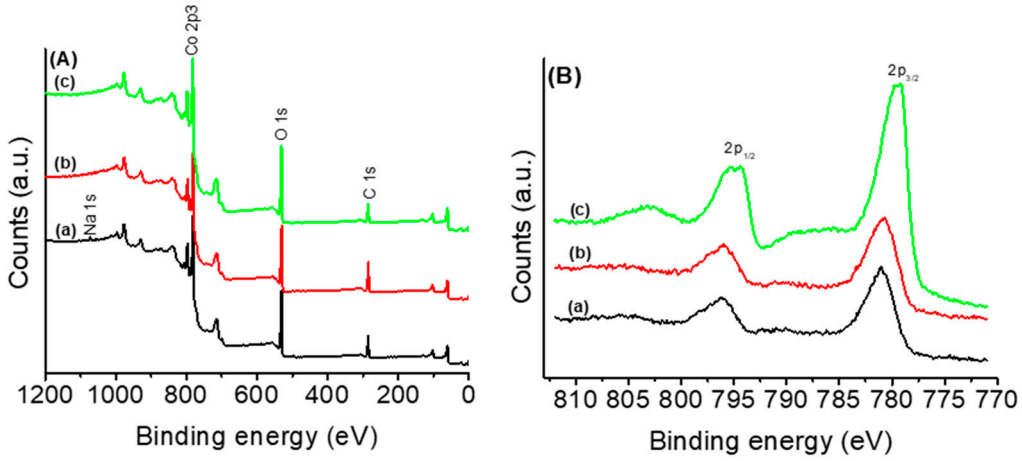

Figure 3. The X-ray photoelectron spectra (XPS) spectra of (a) Co_3O_4, (b) $Co_3O_4(H)$, and (c) CoO(H) catalyst. XPS survey spectra (**A**) and oxidation state (**B**) of samples.

In order to understand the role of Co^{3+}, the activities of CoO(H) catalysts were monitored during PROX reaction at different temperatures. The XPS spectra for Co 2p (A) and O 1s (B) of unspent and spent CoO(H) catalysts (used in CO PROX reaction starting from 40 to 160 °C with an interval of 20 °C) are presented in Figure 4. The observed main peak of Co $2p_{3/2}$ at 779.4 eV and its satellite peak at 785.5 eV (Figure 4, unspent catalyst) indicate that the surface phase of the catalyst is CoO [39,40]. A decrease in intensity of the Co 2p peaks and their satellite peak was observed when the catalyst was used for PROX at 40 °C (Figure 4A), and further decreased with an increase in reactor temperature (up to 100 °C). The XPS data of the catalyst at 100 °C show the absence of the satellite peak, which confirms the formation of a Co_3O_4 spinel structure. These XPS data (Figure 4B) suggest that a transformation from Co^{2+} to Co^{3+} species has occurred, which supports the XRD data (Figure 1f). These findings are supported by the data recorded by Nguyen et al. [10], who noted the presence of a Co_3O_4 spinel structure during PROX. This structural change was also suggested elsewhere under CO oxidation [18]. Interestingly, above 120 °C under PROX, the satellite peak seems to re-emerge, which could be due to the effects of temperature.

The O 1s spectra of CoO(H) (Figure 4B) shows one sharp peak at 529.5 eV and two weak shoulder peaks at 531.2 and 533.3 eV. The high binding energy shoulders are assigned to nonstoichiometric oxygen atoms [41,42] and were defined to be oxygen atoms around oxygen vacancies in the surface lattice [10]. The main peak at 529.5 eV is due to the stoichiometric oxygen atoms of the catalyst surface [10]. Upon exposure to PROX gases, the two shoulder peaks become more visible and remain the same even at higher temperatures. Interestingly, the catalyst spent at 100 °C (Figure 4B) shows that the shoulder peak at 531.2 eV has broadened, while that at 533.0 eV has weakened. This can easily be linked with the formation of a spinel structure, as indicated above. The observed results suggest that the surface oxygen vacancy increased during PROX, which differs from the results reported by Nguyen et al. [10]. This could be due to the H_2 pretreatment temperature, as well as hydrazine treatment effects.

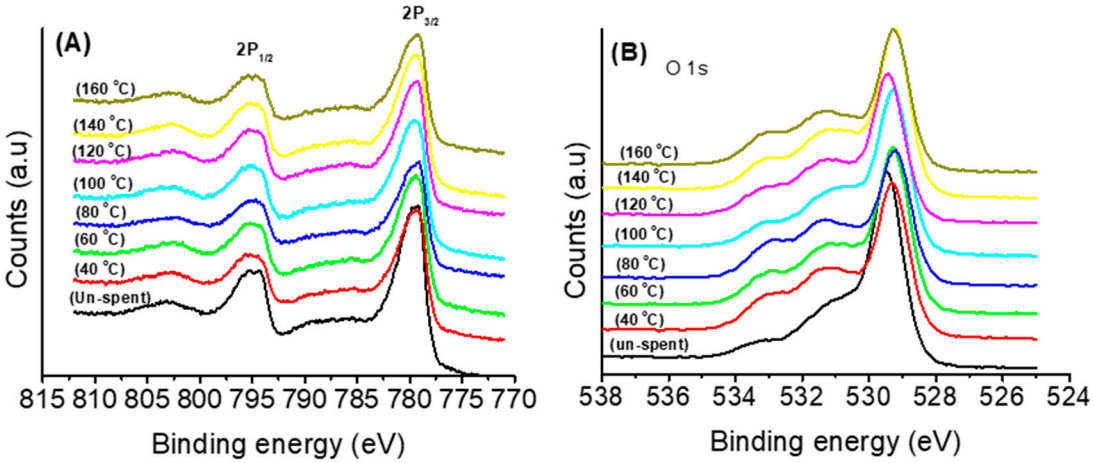

Figure 4. The XPS spectra of (**A**) Co 2p, and (**B**) O 1s of unspent and spent (at different temperatures) CoO(H) catalysts on PROX of CO.

The transformation of the catalysts was further investigated using H_2-TPR, as shown in Figure 5. The Co_3O_4 (Figure 5a) exhibited two main broad peak maxima at 263 °C (with an area of 1260, as shown by the deconvolution of TPR peak, insert) and 326 °C (with an area of 1590), which belong to the stepwise reduction of $Co_3O_4 \rightarrow CoO \rightarrow Co$ [43]. Other researchers have reported a similar reduction trend of Co_3O_4, and this was found to depend on the calcination temperature and the morphology of the materials [44,45]. The reductive pretreatment of the Co_3O_4 by hydrazine (Figure 5b) lowered the reduction maxima from 263 to 220 °C ($Co_3O_4 \rightarrow CoO$). This clearly demonstrated that hydrazine does not eliminate the higher oxidation state of Co_3O_4 but rather changes the surface reducibility of the catalyst. A slight decrease in the peak area (884) of the Co_3O_4(H) (Figure 5b) suggests that a smaller amount of Co^{3+} species was reduced.

The CoO(H) catalyst (Figure 5c) shows an initial broad peak at 204 °C, which can be attributed to the reduction of octahedrally coordinated Co^{3+} species, and the second broad peak with a maximum at 338 °C is attributed to the reduction of tetrahedrally coordinated Co^{2+} species [43]. The TPR of CoO(H) (Figure 5c) indicated the absence of a Co^{3+} peak, as determined by deconvolution of its TPR profile (which gave a negligible amount of area under the peak). The last intense broad peak which shows a reduction profile from 373 to 612 °C is attributed to octahedrally coordinated Co^{2+} species within the CoO(H) catalyst. This indeed confirms that CoO(H) was successfully prepared, and the data is well supported by both XRD and XPS profiles. The TPR profile of a spent CoO(H) (Figure 5d) shows a lower reducibility of the catalyst (at approximately 267 °C, with an area of 1656), which clearly resembles the reduction profile of the Co_3O_4 spinel structure. The overall results suggest that some Co^{2+} (octahedral sites) were converted to Co^{3+} (octahedral sites) during PROX reaction (as relatively confirmed by XRD data). This supports the results reported on CO oxidation [18].

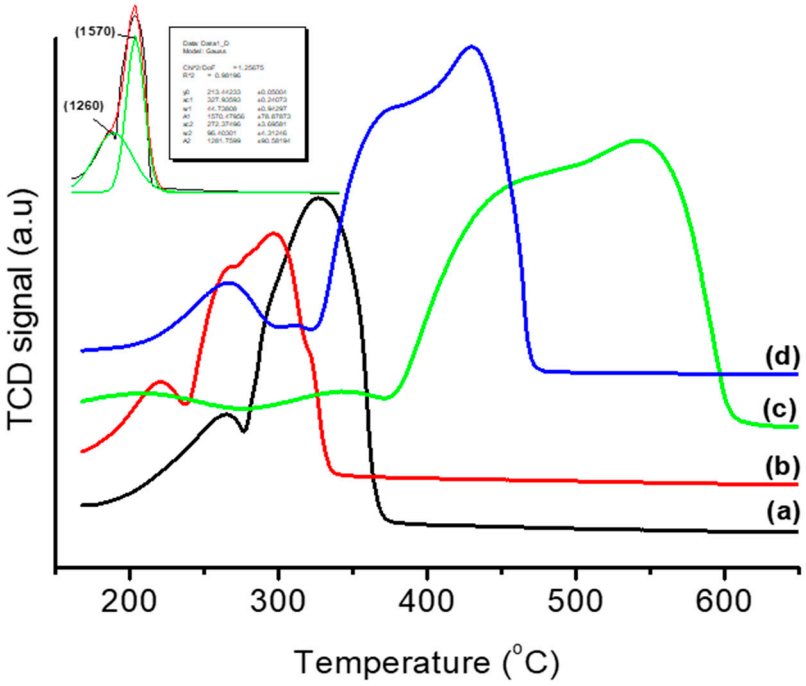

Figure 5. The TPR profiles of (a) Co_3O_4, (b) Co_3O_4(H), (c) CoO(H), and (d) spent CoO(H) catalyst. Insert: Example of deconvoluted TPR peak profile of Co_3O_4.

The FTIR spectra of Co_3O_4, Co_3O_4(H), and CoO(H) samples are shown in Figure 6. The FTIR profile of as-prepared Co_3O_4 and Co_3O_4(H) samples (Figure 6a,b) displayed two distinct and sharp bands at 547 and 651 cm^{-1}, which originate from the stretching vibrations of the metal oxygen bond (Co–O) [35,38]. The band at 547 cm^{-1} is assigned to the octahedral arrangement of Co^{3+}, whilst the band at 651 cm^{-1} is due to Co^{2+} placed in the tetrahedral site [38]. Such an arrangement of Co^{3+} and Co^{2+} ions at octahedral and tetrahedral positions, respectively, confirms the formation of spinel Co_3O_4 phase [46]. This indicates that the same Co_3O_4 phase has been formed upon transformation of CoO_xH_y(H) by calcination, which is consistent with the XRD data. The intensive broad bands at 1630 and 3347 cm^{-1} are due to O–H stretching vibrations, interacting through the H bonds [35]. The formation of CoO(H) is confirmed by the formation of weak bands at 528 and 635 cm^{-1} (Figure 6d), which originate from the stretching vibrations of the metal oxygen bonds (Co–O) [47].

The SEM and TEM images of CoO_xH_y(H), Co_3O_4, Co_3O_4(H) and CoO(H) samples are shown in Figure 7. The SEM image of CoO_xH_y(H) (Figure 7a), indicates the presence of hexagonal platelets and rod-like morphology [48]. The TEM image (Figure 7a1) confirmed the presence of a hexagonal shapes overshadowed by some porous layer [48,49], in agreement with the XRD data. The SEM image of Co_3O_4(H) (Figure 7c) indicated even more formation of hexagonal platelets upon calcination. This image resembles the SEM image of the Co_3O_4 (Figure 7b), although this image shows the presence of a few rod-like morphologies. This suggests somehow that in situ reduction might have assisted in the transformation of rod-like to hexagonal platelet morphology during calcination. The overall structure remained intact, upon reduction by hydrazine, which correlates with the report by Chen et al. [48]. The report by Liu et al. [29] noted an increase in surface roughness of the Co_3O_4, which is in agreement with this paper's SEM and TEM data. Furthermore, the TEM image of both the Co_3O_4 (Figure 7b1) and Co_3O_4(H) samples (Figure 7c1) shows some highly porous aggregates of nanoparticles with a relatively uniform size distribution of 15 to 20 nm. This distribution is well aligned with the XRD data of the two samples. Moreover, the phase identification as shown in Figure 7d indicates the presence of lattice fringe spacing of 0.24 nm (311) [50,51] and 0.28 nm (220), which confirms the characteristic lattice structure of Co_3O_4 [50].

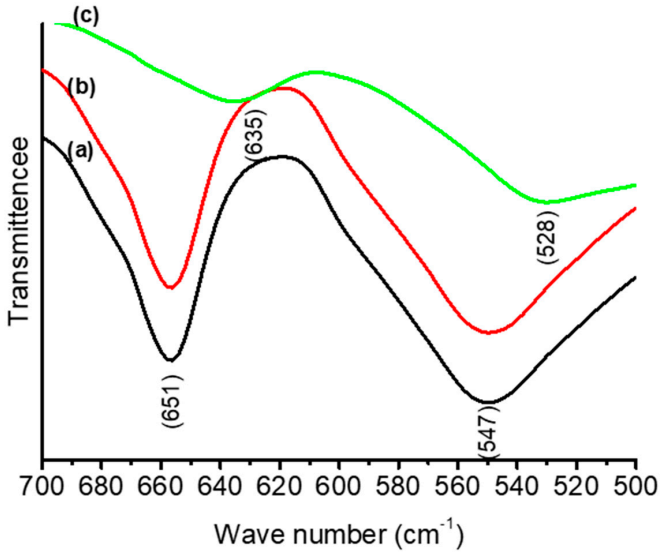

Figure 6. The FTIR spectra of (a) Co_3O_4, (b) Co_3O_4(H), and (c) CoO(H) catalyst.

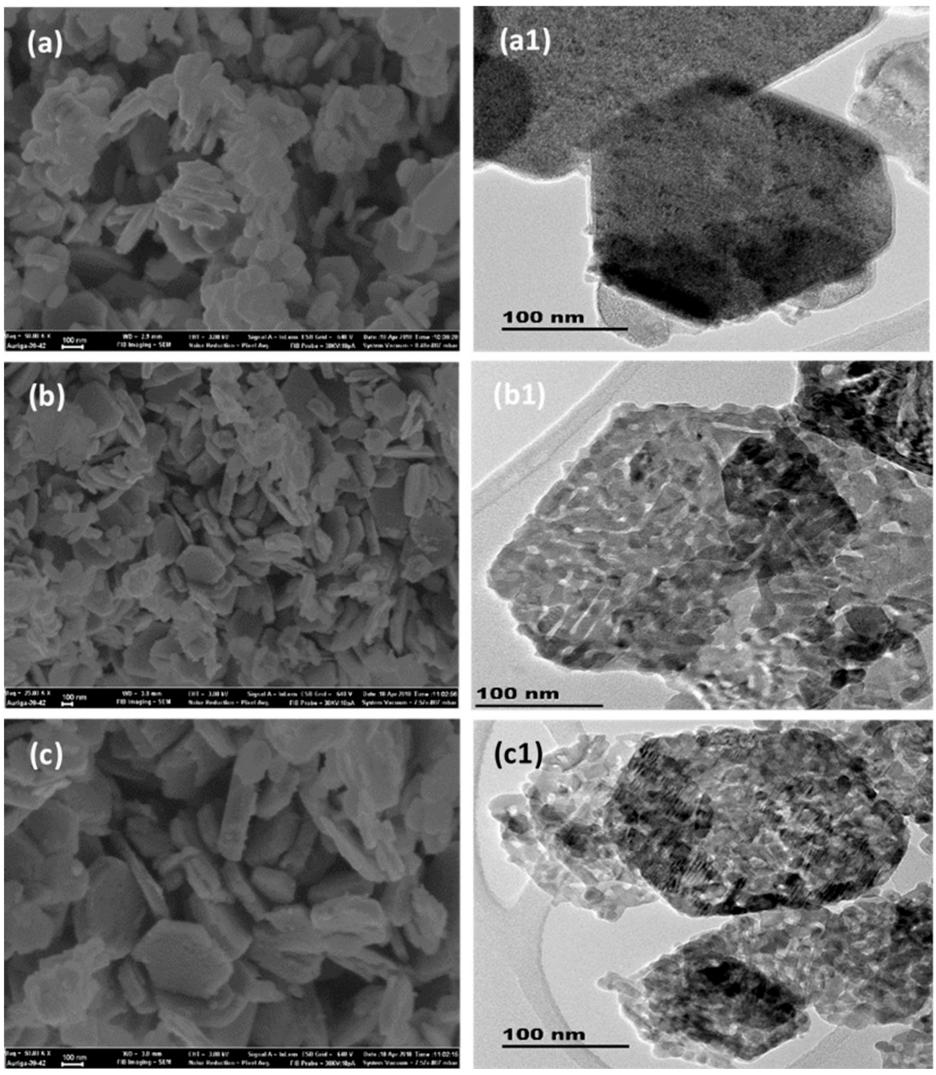

Figure 7. *Cont.*

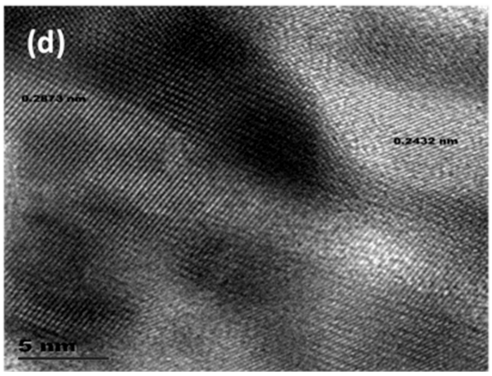

Figure 7. The SEM (**a**, **b**, and **c**) and TEM (**a1**, **b1**, and **c1**) images of (**a**) CoO_xH_y(H), (**b**) Co_3O_4, (**c**) Co_3O_4(H) and (**d**) the high resolution TEM image of Co_3O_4.

3.2. Catalytic Activity for PROX of CO Reaction

3.2.1. Catalytic Performance of Various Cobalt Species on PROX of CO

The data in Figure 8 show the temperature dependence catalytic activities of (a) CoO_xH_y(H), (b) Co_3O_4 and (c) Co_3O_4(H) catalysts for PROX of CO. The CoO_xH_y(H) catalyst (Figure 8Aa) initially showed 18% CO conversion at 40 °C, which then drastically increased to 72% as temperature was increased. The catalyst had a maximum CO conversion at 120 °C. The Co_3O_4 catalyst (Figure 8Ab) showed a lower activity at lower temperature; however, its activity improved with temperature. Eventually, the catalyst had a maximum CO conversion at 160 °C. Such an increase is attributed to a transformation of $Co(OH)_2$ into a spinel Co_3O_4 phase by calcination at 300 °C, as evidenced by structural changes on TEM and SEM data. The TGA profile of as-prepared Co_3O_4 also showed a stable phase within the temperature range, explored on PROX reaction. The catalyst had a slight decrease in conversion and selectivity (Figure 8A, B) above 160 °C, which can be associated with moisture formation [52].

Interestingly, the Co_3O_4(H) catalyst (Figure 8Ac) showed an exponential increase from 40 to 80 °C and a drastic change to 100% conversion at 100 °C, with good selectivity. In situ reduction decreased the maximum CO conversion temperature ($T_{100\%}$) from 160 (over Co_3O_4 catalyst) to 100 °C (Figure 8Ac). The $T_{100\%}$ of standalone Co_3O_4(H) catalyst is well comparable/above (with) the activity of CuO–ceria catalysts, as reported elsewhere [14–17], and better off in terms of selectivity. An average of 98% CO conversion falls within the fuel cells operating temperature window [24]. The PROX activity of the Co_3O_4(H) catalyst is consistent with the suggestion made by Boyd et al. [25], though on different systems (i.e., for the need of partially reduced gold state). Although some in situ reduction has occurred, on the Co_3O_4(H) catalyst, the FTIR data do not show peak ratio differences. Similarly, the XPS results do not provide clear dependents of PROX reaction on the oxidation state of cobalt. However, the TPR data indicate that hydrazine did not completely eliminate the higher oxidation state of Co_3O_4 but improved the surface reducibility/properties of the catalyst.

Several studies [53,54] and a recent finding [48] have attributed an enhanced activity of *p*-nitrophenol reduction over the reduced Co_3O_4 catalyst, to the oxygen vacancies created during surface reduction process. It is therefore expected that the high PROX activity observed over Co_3O_4(H) could easily be associated with the created oxygen vacancies [55]. In addition to the oxygen vacancy created, the BET data showed an improved specific surface area and pore volume (Table 1) upon reduction. The catalyst had almost 100% selectivity to CO_2 from 40 to 120 °C, which was followed by almost 6% decrease at 140 °C (Figure 8Bc). The catalyst showed almost zero H_2 conversion and selectivity towards moisture (Figure 8C,D). The Co_3O_4(H) catalyst outperformed the PROX activity of the Co_3O_4–CeO_2 catalyst reported by Arango-Diaz et al. [24]. This reduces the needs of bimetallic oxides catalysts, which could result in lower catalyst costs.

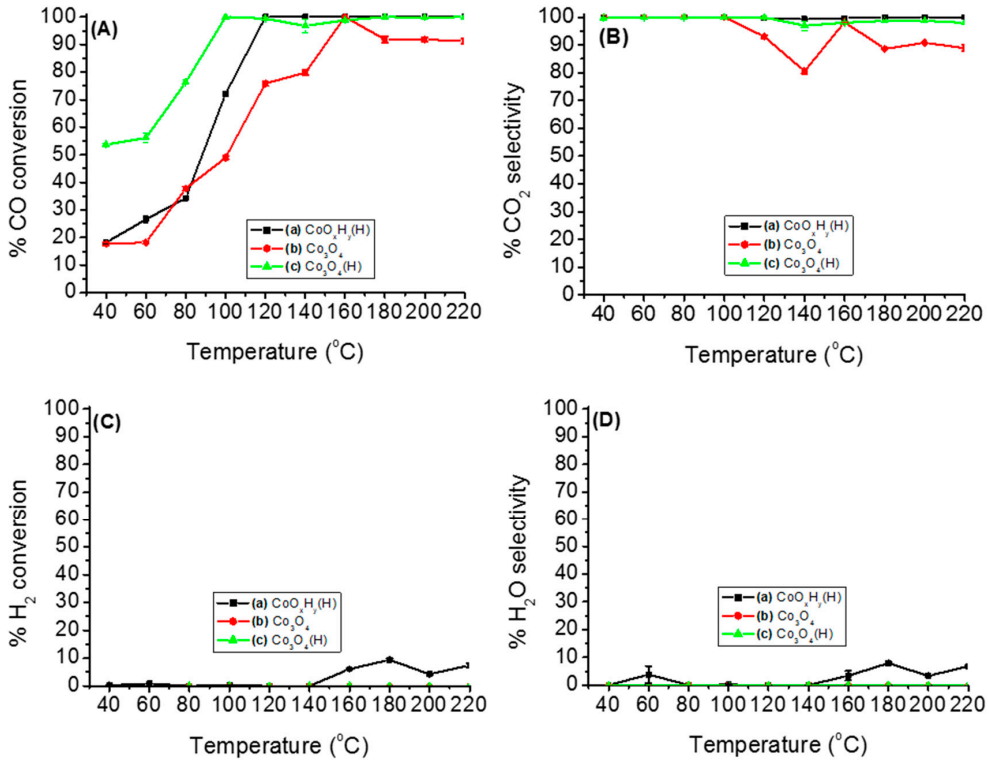

Figure 8. The CO conversion (**A**), CO_2 selectivity (**B**), H_2 conversion (**C**), and H_2O selectivity (**D**) of (a) $CoO_xH_y(H)$ (■), (b) Co_3O_4 (●), and (c) $Co_3O_4(H)$ (▲) catalysts.

Furthermore, in order to understand the origin of the PROX activity of the $Co_3O_4(H)$ catalyst, a comparison was conducted using the as-prepared CoO and CoO(H) catalysts (this was achieved by further reducing the $Co_3O_4(H)$ catalyst in 5% H_2/He at 250 °C, as indicated under methodology). Interestingly, the data show that the formed CoO(H) catalyst (Figure 9Ac) performed better than both pure CoO (Figure 9Aa) and $Co_3O_4(H)$ (Figure 9Ab) at a low temperature region. However, the activities of the three catalysts were also comparable at higher temperatures. The higher activity of CoO(H) is attributed to its transformation to Co_3O_4 upon exposure to PROX gases (starting from 40 °C). This was clearly demonstrated by XPS data, which indicated a transformation of octahedrally coordinated Co^{2+} species to octahedrally coordinated Co^{3+} species (in the presence of PROX gases). This was further confirmed by the TPR and XRD profiles of spent CoO(H) catalyst. This behavior supports the reported oxidation of an octahedral Co^{2+} species, which resulted in high CO oxidation [18].

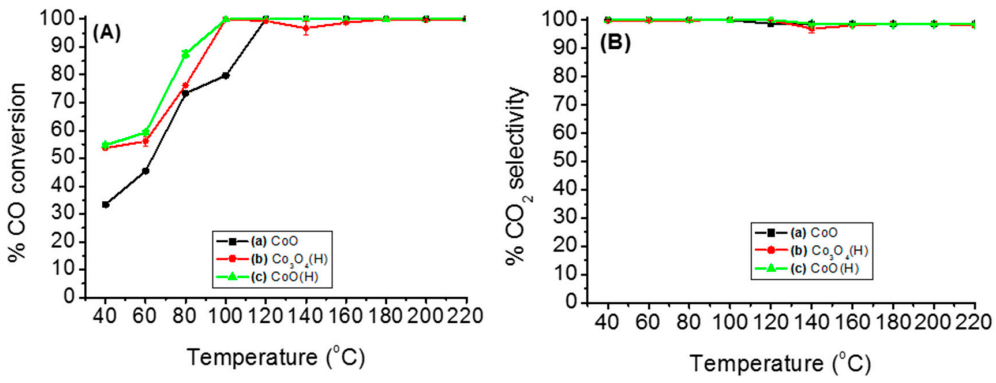

Figure 9. The CO conversion (**A**) and CO_2 selectivity (**B**) of (a) CoO (■), (b) $Co_3O_4(H)$ (●), and (c) CoO(H) (▲) catalysts.

3.2.2. Effects of Temperature, Moisture and CO_2 on the Stability of Either Co_3O_4 or Co_3O_4(H)

The results for the effects of temperature, moisture (by bubbling He gas through water vessel at 20 mL·min^{-1}, at room temperature), and CO_2 in the feed are presented in Figure 10. The Co_3O_4 catalyst gave approximately 68% CO conversion, which deactivated with time on stream at 100 °C for 21 h (Figure 10Ba). However, the Co_3O_4(H) catalyst produced 100% CO conversion, which remained the same for almost an hour (Figure 10Bb). Thereafter, the catalyst activity decreased to 85% (after 160 min), which was accompanied by steady fluctuations for almost 21 h (Figure 10Bb). Interestingly, as a function of temperature (Figure 10A), the introduction of moisture in the feed of Co_3O_4(H) gave almost the same activity as that of the dry condition. The activities of this catalyst remained almost unchanged (for a temperature up to 220 °C), which indicates very good stability. However, when the catalyst operated on stream at 100 °C (Figure 10Bc), it immediately deactivated from 100% to approximately 70% CO conversion and remained fluctuating steadily for almost 21 h. These data are consistent with the report by Li et al. [27], who noted a stable and high CO oxidation at high temperatures, hence avoiding the phenomenon of H_2O capillary condensation. The stability of Co_3O_4(H) under a dry condition can well be attributed to in situ reduction as compared to the Co_3O_4 catalyst, which seems to lose activity much faster.

The catalytic activity of the Co_3O_4(H) catalyst in the presence of 15% CO_2 in the feed showed a sudden decrease from 75% CO conversion within 5 min at 100 °C (Figure 10Bd). As time progressed, a steady decrease to 27% CO conversion was observed. The decrease in CO conversion can be associated with a competitive effect between CO and CO_2 that hinders the redox circle Co^{3+}–Co^{2+} [24].

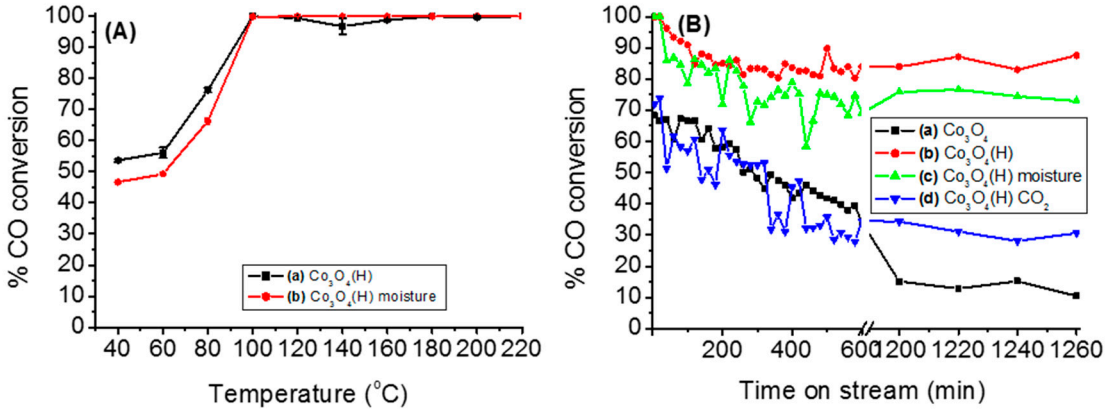

Figure 10. The effects of moisture as a function of temperature (**A**) and time on stream at 100 °C (**B**): Effects of moisture (c) and CO_2 (d) on the stability of either Co_3O_4 (■), or Co_3O_4(H) (●) (B).

4. Conclusions

The Co_3O_4 and Co_3O_4(H) catalysts were successfully prepared using the precipitation method prior to calcination at 300 °C. Both the CoO and CoO(H) catalysts were prepared by reducing Co_3O_4 and Co_3O_4(H) by 5%H_2/He, respectively. The structural compositions of the catalysts were confirmed by XRD, FTIR, XPS, TPR, and TGA data, with the activity of the catalysts investigated under PROX reaction. The XRD and TPR data of the Co_3O_4(H) catalyst indicated that a surface transformation occurred, as confirmed by an increase in the BET surface area. Interestingly, the mesoporous structure of the catalyst remained intact, as compared to that of the Co_3O_4 catalyst.

The PROX data of Co_3O_4(H) catalyst had 85% CO conversion (with good selectivity) at 100 °C, under dry conditions, which remained stable for over 21 h. The catalyst activity increased with temperature, especially within the fuel cells temperature window. This activity correlated with the surface properties of the catalyst and showed a very low moisture formation at temperatures above 120 °C. A relatively similar activity with good stability was observed under a moisture-rich

condition, avoiding the H_2O capillary condensation phenomenon. The data indicated that the Co_3O_4 catalyst is unstable and deactivated with time on stream at 100 °C. The PROX activity of the Co_3O_4(H) catalyst in the presence of moisture deactivated from 100 to 70% and remained fluctuating steadily for almost 21 h. The Co_3O_4(H) produced approximately 75% CO conversion in the presence of CO_2, which deactivated as time increased. Surprisingly, the PROX of CoO(H) indicated that the catalyst is highly active at a low temperature range, which correlated with the formation of Co^{3+} species as confirmed by TPR and XRD data.

Author Contributions: R.M. performed the experiments, analysed the data, interpreted the data and wrote the first draft. T.M. (Thuto Musuang) was responsible for proof reading and interpretation of the data. T.M. (Takalani Magadzu) designed the project and experiments, revised the data interpretation and contributed to the discussion and paper structure. All authors contributed to the organisation and refining of the manuscript.

Funding: This research was funded by National Research Foundation (NRF), Grant number: UID 105181, and University of Limpopo staff development grant.

Acknowledgments: The support of this work by the National Research Foundation (NRF) and University of Limpopo, Department of Chemistry is gratefully acknowledged. The work was presented at the 43rd South African Chemical Institute (SACI) National Conversion in December of 2018 (with no restrictions on publication).

Conflicts of Interest: We declare that there are no conflicts of interest with regard to the publication of this paper.

References

1. Abdollah, M.; Yu, J.P.; Liu, K.T.; Ciora, R.; Sahimi, M.; Tsotsis, T.T. Ultra-pure hydrogen production from reformate mixtures using a palladium membrane reactor system. *J. Membr. Sci.* **2012**, *390–391*, 32–42. [CrossRef]
2. Sedmak, G.; Hocevar, S.; Levec, J. Kinetics of selective CO oxidation in excess of H_2 over the nanostructured $Cu_{0.1}Ce_{0.9}O_{2-y}$ catalyst. *J. Catal.* **2003**, *213*, 135–150. [CrossRef]
3. Park, J.W.J.; Jeong, H.; Yoon, W.L.C.; Kim, S.D.; Lee, K.; Park, Y.; Rhee, Y. Selective oxidation of CO in hydrogen-rich stream over Cu–Ce catalyst promoted with transition metals. *Int. J. Hydrogen Energy* **2005**, *30*, 209–220.
4. Korotkikh, O.; Farrauto, R. Selective catalytic oxidation of CO in H_2: Fuel cell applications. *Catal. Today* **2000**, *62*, 249–254. [CrossRef]
5. Nguyen, T.-S.; Morfin, V.; Aouine, V.; Bosset, V.; Rousset, J.-L.; Piccolo, L. Trends in the CO oxidation and PROX performances of the platinum-group metals supported on ceria. *Catal. Today* **2015**, *253*, 106–114. [CrossRef]
6. Miguel-García, I.; Berenguer-Murcia, Á.; Cazorla-Amorós, D. Preferential oxidation of CO catalyzed by supported polymer-protected palladium-based nanoparticles. *Appl. Catal. B Environ.* **2010**, *98*, 161–170. [CrossRef]
7. Jardim, E.O.; Goncalves, M.; Rico-Francés, S.; Sepúlveda-Escribano, A.; Silvestre-Albero, J. Superior performance of multi-wall carbon nanotubes as support of Pt-based catalysts for the preferential CO oxidation: Effect of ceria addition. *Appl. Catal. B Environ.* **2012**, *113–114*, 72–78. [CrossRef]
8. Rossignol, C.; Arrii, S.; Morfin, F.; Piccolo, L.; Caps, V.; Rousset, J.-L. Selective oxidation of CO over model gold-based catalysts in the presence of H_2. *J. Catal.* **2005**, *230*, 476–483. [CrossRef]
9. Reina, T.R.; Megías-Sayago, C.; Florez, A.P.; Ivanova, S.S.; Centeno, S.J.; Odriozola, A. H_2 oxidation as criterion for PrOx catalyst selection: Examples based on Au–CoO_x-supported systems. *J. Catal.* **2015**, *326*, 161–171. [CrossRef]
10. Nguyen, L.; Zhang, S.; Yoon, S.J.; Tao, F. Preferential Oxidation of CO in H_2 on Pure Co_3O_4-x and Pt/Co_3O_4-x. *ChemCatChem* **2015**, *7*, 2346–2353. [CrossRef]
11. Pozdnyakoya, O.; Tescher, D.; Wootsch, A.; Krohnert, J.; Steinhauer, B.; Sauer, H.; Toth, L.; Jentoft, F.C.; Knop-Gericke, A.; Paal, Z.; et al. Preferential CO oxidation in hydrogen (PROX) on ceria-supported catalysts, part II: Oxidation states and surface species on Pd/CeO_2 under reaction conditions, suggested reaction mechanism. *J. Catal.* **2006**, *237*, 17–28. [CrossRef]
12. Marino, F.; Descorme, F.; Dupre, D. Noble metal catalysts for the preferential oxidation of carbon monoxide in the presence of hydrogen (PROX). *Appl. Catal. Environ.* **2004**, *54*, 59–66. [CrossRef]

13. Zlotea, C.; Morfin, F.; Nguyen, T.S.; Nguyen, N.T.; Nelayah, J.; Ricolleau, C.; Latroche, M.; Piccolo, L. Nanoalloying bulk-immiscible iridium and palladium inhibits hydride formation and promotes catalytic performances. *Nanoscale* **2014**, *6*, 9955–9959. [CrossRef] [PubMed]
14. Marba'n, G.; Fuertes, A.B. Highly active and selective CuO_x/CeO_2 catalyst prepared by a single-step citrate method for preferential oxidation of carbon monoxide. *Appl. Catal. B Environ.* **2005**, *57*, 43–53. [CrossRef]
15. Gong, X.; Liu, B.; Kang, B.; Xu, G.; Wang, Q.; Jia, C.; Zhang, J. Boosting Cu-Ce interaction in Cu_xO/CeO_2 nanocube catalysts for enhanced catalytic performance of preferential oxidation of CO inH_2-rich gases. *Mol. Catal.* **2017**, *436*, 90–99. [CrossRef]
16. Zhu, C.; Ding, T.; Gao, W.; Ma, K.; Tian, Y.; Li, X. CuO/CeO_2 catalysts synthesized from Ce-UiO-66 metal-organic framework for preferential CO oxidation. *Int. J. Hydrogen Energy* **2017**, *42*, 17457–17465. [CrossRef]
17. Di Benedetto, A.; Landi, G.; Lisi, L. Improved CO-PROX performance of CuO/CeO_2 catalysts by using nanometric ceria as support. *Catalysts* **2018**, *8*, 209. [CrossRef]
18. Gu, D.; Jia, C.-J.; Weidenthaler, C.; Bongard, H.-J.; Spliethoff, B.; Schmidt, W.; Schüth, F. Highly Ordered Mesoporous Cobalt-Containing Oxides: Structure, Catalytic Properties, and Active Sites in Oxidation of Carbon Monoxide. *J. Am. Chem. Soc.* **2015**, *137*, 11407–11418. [CrossRef]
19. Teng, Y.; Skurai, H.; Ueda, A.; Kobayashi, T. Oxidative removal of CO contained in hydrogen by using metal oxide catalysts. *Int. J. Hydrogen Energy* **1999**, *24*, 355–358. [CrossRef]
20. Lukashuk, L.; Föttinger, K.; Kolar, E.; Rameshan, C.; Teschner, D.; Hävecker, M.; Knop-Gericke, A.; Yigit, N.; Li, H.; McDermott, E.; et al. Operando XAS and NAP-XPS studies of preferential CO oxidation on Co_3O_4 and CeO_2-Co_3O_4 catalysts. *J. Catal.* **2016**, *344*, 1–15. [CrossRef]
21. Broqvist, P.; Panas, I.; Persson, H.A. A DFT Study on CO Oxidation over Co_3O_4. *J. Catal.* **2002**, *210*, 198–206. [CrossRef]
22. Umegaki, T.; Inoue, T.; Kojima, Y. Fabrication of hollow spheres of Co_3O_4 for catalytic oxidation of carbon monoxide. *J. Alloys Compd.* **2016**, *663*, 68–76. [CrossRef]
23. Jansson, J.; Palmqvist, A.E.C.; Fridell, E.; Skoglundh, M.; Österlund, L.; Thormählen, P.; Langer, V. On the Catalytic Activity of Co_3O_4 in Low-Temperature CO Oxidation. *J. Catal.* **2002**, *211*, 387–397. [CrossRef]
24. Arango-Diaz, A.; Cecilia, J.A.; Marrero-Jerez, J.; Nuñez, P.; Jiménez-Jiménez, J.; Rodríguez-Castellón, E. Freeze-dried Co_3O_4–CeO_2 catalysts for the preferential oxidation of CO with the presence of CO_2 and H_2O in the feed. *Ceram. Int.* **2016**, *42*, 7462–7474. [CrossRef]
25. Boyd, D.; Golunski, S.; Hearne, G.R.; Magadzu, T.; Mallick, K.; Raphulu, M.C.; Venugopal, A.; Scurrell, M.S. Reductive routes to stabilized nano gold and relation to catalysis by supported gold. *Appl. Catal. A Gen.* **2005**, *292*, 76–81. [CrossRef]
26. Lakshmanan, P.; Park, J.E.; Kim, B.; Park, E.D. Preferential oxidation of CO in a hydrogen-rich stream over $Au/MO_x/Al_2O_3$(M = La, Ce, and Mg) catalysts. *Catal. Today* **2016**, *265*, 19–26. [CrossRef]
27. Li, G.; Li, L.; Yuan, Y.; Shi, J.; Yuan, Y.; Li, Y.; Zhao, W.; Shi, J. Highly efficient mesoporous Pd/CeO_2catalyst for low temperature CO oxidation especially under moisture condition. *Appl. Catal. B Environ.* **2014**, *158–159*, 341–347. [CrossRef]
28. Chen, Y.; Liu, D.; Yang, L.; Meng, M.; Zhang, J.; Zheng, L.; Chu, S.; Hu, T. Ternary composite oxide catalysts CuO/Co_3O_4–CeO_2 with wide temperature-window for the preferential oxidation of CO in H_2-rich stream. *Chem. Eng. J.* **2013**, *234*, 88–98. [CrossRef]
29. Liu, Y.-C.; Koza, J.A.; Switzer, J.A. Conversion of electrodeposited $Co(OH)_2$ to CoOOH and Co_3O_4, and comparison of their catalytic activity for the oxygen evolution reaction. *Electrochim. Acta* **2014**, *140*, 359–365. [CrossRef]
30. Farhadi, S.; Pourzare, K.; Sadeghinejad, S. Synthesis and characterization of Co_3O_4 nanoplates by simple thermolysis of the $[Co(NH_3)_6]_2(C_2O_4)_3$-$4H_2O$ complex. *Polyhedron* **2014**, *67*, 104–110. [CrossRef]
31. Kaviyarasu, K.; Raja, A.; Devarajan, P.A. Structural elucidation and spectral characterizations of Co_3O_4 nanoflakes. *Spectrochim. Acta Part A Mol. Biomol. Spectrosc.* **2013**, *114*, 586–591. [CrossRef] [PubMed]
32. Sharifi, S.L.; Shakur, H.R.; Mirzaei, A.; Salmani, A.; Hosseini, M.H. Characterization of Cobalt Oxide Co_3O_4 Nanoparticles Prepared by Various Methods: Effect of Calcination Temperatures on Size, Dimension and Catalytic Decomposition of Hydrogen Peroxide. *Int. J. Nanosci. Nanotechnol.* **2013**, *9*, 51–58.

33. Li, G.; Li, L.; Shi, J.; Yuan, Y.; Li, Y.; Zhao, W.; Shi, J. One-pot pyrolytic synthesis of mesoporous $MCo_2O_{4(4.5)}$ (M = Mn, Ni, Fe, Cu) spinels and its high efficient catalytic properties for CO oxidation at low temperature. *J. Mol. Catal. A Chem.* **2014**, *390*, 97–104. [CrossRef]
34. Tang, C.-W.; Hsu, L.-C.; Yu, S.-W.; Wang, C.-B.; Chien, S.-H. In situ FT-IR and TPD-MS study of carbon monoxide oxidation over a CeO_2/Co_3O_4 catalyst. *Vib. Spectrosc.* **2013**, *65*, 110–115. [CrossRef]
35. Ozkaya, T.; Baykal, A.; Toprak, M.S.; Koseoglu, Y.; Durmus, Z. Reflux synthesis of Co_3O_4 nanoparticles and magnetic characterisation. *J. Magn. Magn. Mater.* **2009**, *321*, 2145–2149. [CrossRef]
36. Jayashree, R.S.; Kamath, V.P. Electrochemical synthesis of a-cobalt hydroxide. *J. Chem.* **1999**, *9*, 961–963. [CrossRef]
37. Barde´, F.; Palacin, M.-R.; Beaudoin, B.; Delahaye-Vidal, A.; Tarascon, J.-M. New Approaches for Synthesizing çIII-CoOOH by Soft Chemistry. *Chem. Mater.* **2004**, *16*, 299–306. [CrossRef]
38. Tang, C.W.; Wang, C.B.; Chien, S.H. Characterization of cobalt oxides studied by FT-IR, Raman, TPR and TG-MS. *Thermochim. Acta* **2008**, *473*, 68–73. [CrossRef]
39. Natile, M.M.; Glisenti, A. CoO_x/CeO_2 Nanocomposite Powders: Synthesis, Characterization, and Reactivity. *Chem. Mater.* **2005**, *17*, 3403–3414. [CrossRef]
40. Mate, V.R.; Jha, A.; Joshi, U.D.; Patil, K.R.; Shirai, M.; Rode, C.V. Effect of preparation parameters on characterization and activity of Co_3O_4 catalyst in liquid phase oxidation of lignin model substrates. *Appl. Catal. A Gen.* **2014**, *487*, 130–138. [CrossRef]
41. Zhang, S.; Shan, J.-J.; Zhu, Y.; Frenkel, A.I.; Patlolla, A.; Huang, W.; Yoon, S.J.; Wang, L.; Yoshida, H.; Takeda, S.; et al. WGS Catalysis and in Situ Studies of CoO_{1-x}, PtCon/Co_3O_4, and PtmCom′/CoO_{1-x} Nanorod Catalysts. *J. Am. Chem. Soc.* **2013**, *135*, 8283–8293. [CrossRef] [PubMed]
42. Wang, L.; Zhang, S.; Zhu, Y.; Patlolla, A.; Shan, J.; Yoshida, H.; Takeda, S.; Frenkel, A.I.; Tao, F. Catalysis and In Situ Studies of Rh1/Co_3O_4 Nanorods in Reduction of NO with H_2. *Acta Catal.* **2013**, *3*, 1011–1019. [CrossRef]
43. Tang, Y.; Ma, L.; Dou, J.; Andolina, C.M.; Li, Y.; Ma, H.; House, S.D.; Zhan, X.; Yang, J.; Tao, F. Transition of surface phase of cobalt oxide during CO oxidation. *Phys. Chem. Chem. Phys.* **2018**, *20*, 6440–6449. [CrossRef] [PubMed]
44. Chang, T.; Shen, Z.; Huang, Y.; Lu, J.; Ren, D.; Cao, J.; Liu, H. Post-plasma-catalytic removal of toluene using MnO_2–Co_3O_4 catalysts and their synergistic mechanism. *Chem. Eng. J.* **2018**, *348*, 15–25. [CrossRef]
45. Nidhin, M.; Sreeram, K.J.; Nair, B.U. Green synthesis of rock salt CoO nanoparticles for coating applications by complexation and passivation with starch surface. *Chem. Eng. J.* **2012**, *185–186*, 352–357. [CrossRef]
46. de la Pena O'Shea, V.A.; Homs, N.; Pereira, E.B.; Nafria, R.; de la Piscina, P.R. X-ray diffraction study of Co_3O_4 activation under ethanol steam-reforming. *Catal. Today* **2007**, *126*, 148–152. [CrossRef]
47. Xu, Z.P.; Zeng, H.C. Interconversion of Brucite-like and Hydrotalcite-like Phases in Cobalt Hydroxide Compounds. *Chem. Mater.* **1999**, *11*, 67–74. [CrossRef]
48. Chen, H.; Yang, M.; Tao, S.; Chen, G. Oxygen vacancy enhanced catalytic activity of reduced Co_3O_4 toward sp-nitrophenol reduction. *Appl. Catal. B Environ.* **2017**, *209*, 648–656. [CrossRef]
49. Yang, J.; Liu, H.; Martens, V.; Frost, R.L. Synthesis and characterization of Cobalt Hydroxide, Cobalt Oxyhydroxide, and Cobalt Oxide Nanodiscs. *J. Phys. Chem. C* **2010**, *114*, 111–119. [CrossRef]
50. Yang, J.; Quaresma, S.; Mei, S.; Ferreira, J.M.F. Hydrothermal synthesis of free-standing Co_3O_4 nanocubes. *Key Eng. Mater.* **2005**, *280–283*, 713–716.
51. Mahammadunnisa, S.K.; Akanksha, T.; Krushnamurty, K.; Subrahmanyam, C.H. Catalytic decomposition of N_2O over CeO_2 supported Co_3O_4 catalysts. *J. Chem. Sci.* **2016**, *128*, 1795–1804. [CrossRef]
52. Jia, C.-J.; Schwickardi, M.; Weidenthaler, C.; Schmidt, W.; Korhonen, S.; Weckhuysen, B.M.; Schüth, F. Co_3O_4-SiO_2 Nanocomposite: A Very Active Catalyst for CO Oxidation with Unusual Catalytic Behavior. *J. Am. Chem. Soc.* **2011**, *133*, 11279–11288. [CrossRef] [PubMed]
53. Liotta, L.F.; Di Carlo, G.; Pantaleo, G.; Venezia, A.M.; Deganello, G. Co_3O_4/CeO_2 composite oxides for methane emissions abatement: Relationship between Co_3O_4–CeO_2 interaction and catalytic activity. *Appl. Catal. B Environ.* **2006**, *66*, 217–227. [CrossRef]

54. Li, J.-B.; Jiang, Z.-Q.; Qianb, K.; Huang, W.-X. Effect of calcination temperature on surface oxygen vacancies and catalytic performance towards CO oxidation of Co_3O_4 nanoparticles supported on SiO_2. *Chin. J. Chem. Phys.* **2012**, *25*, 103–109. [CrossRef]
55. Mei, J.; Ke, Y.; Yu, Z.; Hu, X.; Qu, Z.; Yan, N. Morphology-dependent properties of Co_3O_4/CeO_2 catalysts for low temperature dibromomethane (CH_2Br_2) oxidation. *Chem. Eng. J.* **2017**, *320*, 124–134. [CrossRef]